Materials and Design 176 (2019) 107827

Contents lists available at ScienceDirect

Materials and Design

journal homepage: www.elsevier.com/locate/matdes

Performance indices and selection of thin hard coatings on soft substrates for indentation and scratch resistance

Audrey Favache [a,*], Alain Daniel [b], Aline Teillet [c,1], Thomas Pardoen [a]

[a] Institute of Mechanics, Materials and Civil Engineering, UCLouvain, Place Sainte Barbe 2 – L5.02.02, 1348 Louvain-la-Neuve, Belgium
[b] CRM Group, Avenue du Bois Saint Jean 21, 4000 Liege, Belgium
[c] Coatings Research Institute, Limelette, Belgium

HIGHLIGHTS

- Closed form mechanical models for assessing the scratch resistance of hard film on soft substrate are developed.
- Models for substrate plasticity and film cracking are based on plate theory and validated by finite element simulations.
- Performance indices are proposed for ranking "hard film on soft substrate" systems with respect to scratch resistance.
- Illustrative material property charts compare the protective capacity of some usual thin coating systems.

GRAPHICAL ABSTRACT

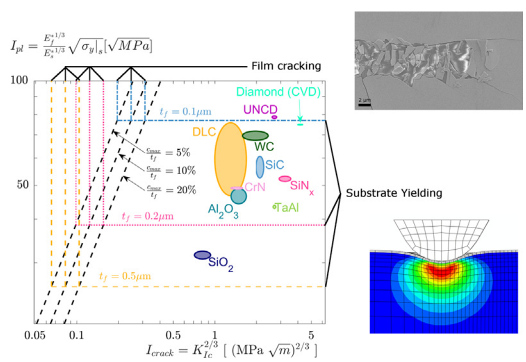

ARTICLE INFO

Article history:
Received 22 February 2019
Received in revised form 17 April 2019
Accepted 2 May 2019
Available online 3 May 2019

Keywords:
Property maps
Thin films
Indentation
Scratch

ABSTRACT

A generic mechanical framework has been developed for assessing the indentation and scratch resistance of hard films on soft substrates. Analytical expressions for the critical loads leading to film cracking or substrate yielding are proposed based on closed form plate bending models and on finite element simulations. These models lead to the definition of performance indices for the ranking of "hard-film-on-soft-substrate" systems with respect to the resistance to indentation and scratch failure under the constraint of minimizing film thickness. These performance indices show that the hardest coating is not always the best choice and that other material properties of the film and the substrate have to be taken into account. An illustrative material property chart is proposed in order to compare the protective ability of some usual thin coatings. These results constitute a guide for the development of layered systems in order to avoid time consuming and expensive trial and error campaigns.

1. Introduction

The need for more efficient multilayer coatings is a collateral effect of the current trend for the development of new high performance multi-functionalized surfaces. Beside the primary functionalities, the long-term reliability of the associated devices relies on the resistance to failure. The mechanical behavior of multilayers is far from being dictated by a simple law of mixture of the single layer behaviors, especially when

* Corresponding author.
E-mail address: Audrey.favache@uclouvain.be (A. Favache).
[1] Present address: Axelera, Rond-point de l'échangeur, Les Levées, 69360 SOLAIZE, France.

https://doi.org/10.1016/j.matdes.2019.107827

dealing with abrasion, scratch and wear resistance. The link between the tribological behavior and the fundamental material properties of the layers is still a subject of research. However, the research and the development of new coatings or new multilayers heavily need tools for selecting the most promising candidates or for orienting material research towards better systems, and this, in order to avoid time consuming and expensive trial and error campaigns.

The main objective of the paper is to propose a simple and easily understandable mechanical approach for assessing the indentation, abrasion and scratch resistance of coated systems. The methodology is inspired from the study described in reference [1] which addressed bulk materials only. Idealized contact scenarios leading to different damage mechanisms are considered. The goal is to derive analytical damage criteria based on which the material selection approach popularized by M. Ashby can be applied [2]. In this methodology, an objective is defined as a function of the desired application, e.g. in terms of minimum cost or weight, and/or maximum the failure load. This objective has to be optimized under constraints, e.g. transparency, electrical conductivity… The analytical evaluation of the objective optimum under constraint leads to the expression of *performance indices*, which are combinations of material properties. Charts can then be built based on the performance indices to guide the best material solution. These indices constitute a measure of the resistance of the system to one type of damage and can be used to classify the different systems as already successfully applied in numerous applications [3–7].

The systems under interest in this study are composed of a thin brittle coating deposited on a comparatively soft layer, typically a polymer. This soft layer can be the substrate or a thick interlayer deposited on another substrate. Applications in which such "hard-on-soft" multilayer stacks are used encompass, among others, surface protection (paints), advanced optics or novel flexible electronics applications (see e.g. [8,9]). Different failure modes during indentation or sliding contact may take place depending on the different materials in the stack such as film cracking, permanent groove formation or film decohesion. Examples of scratch induced failure classifications are given in [10,11] and references [12–14] show experimental results of scratching of thin hard films on soft substrates. Although we are dealing with scratch conditions in this work, all the results may be applied to ball-on-disc testing, since the solicitation is almost the same.

Contrary to bulk materials, analytical relationships providing the critical loads associated to scratch failure mechanisms in coatings are not much addressed in the literature. One of the reasons is the extreme complexity of the mechanical fields below a contact on a stack of material layers possibly involving plasticity. The literature has focused on the deconvolution of substrate effects in hardness measurements [15–18]. However, in order to derive performance indices, the stress field (or at least the maximum stress indicator that leads to failure) must be known in addition to the global response. Gerberich et al. [19] and Bahr [20] provided analytical models of "hard layer-on-soft substrate" indentation. They derived a load-displacement relationship as well as local stresses by considering the film as a membrane bent elastically into a compliant substrate. These models are valid only during substrate yielding whereas the interest here is to determine the first failure mode, i.e. the onset of substrate yielding. Modelling the film as an elastic plate resting on an elastic foundation and deforming mainly due to bending (such as in [21,22]) suits better the objective. Winkler's model [23,24] and Hogg's model [25] have been initially formulated for civil engineering applications in order to address concrete slabs resting on soil. Although differing in the underlying assumptions, the two models result in the same expression for the evolution of the maximum displacement with the load. Winkler's model represents the substrate as a system of mutually independent linear elastic springs. The deflection at one point is independent of the reaction forces elsewhere. This is valid for a floating plate but it is a crude assumption if the film and the substrate are bonded as in the present problem. Contrarily, Hogg considers a bonded plate. Other studies, such as references [26, 27], focused on film fracture, giving expressions for the stress intensity factor associated to a cracked configuration based on finite element simulations.

In this work, we focus on two competing damage scenarios:

1. Plastic yielding of the soft substrate: often, the hard layer has a protective purpose, preventing the soft layer to undergo plastic deformation. The performance index will be derived by determining the critical force on the indenting tip, which leads to plastic deformation in the substrate.
2. Fracture of the hard film: several studies have shown that brittle films on soft substrates indented by a sphere undergo through-thickness fracture [20–22,28]. Moreover, the through-thickness cracking of the film is one of the possible damage modes observed when scratching brittle films on ductile substrates [29]. The performance index is derived by determining the critical force that leads to the cracking of the film.

For these two damage modes, simple material selection criteria are proposed. These criteria take both the film and the substrate into account, which is not the case in studies like the one in reference [30], for instance, which consider only the film material.

The paper is organized as followed. Simplified analytical models are proposed in Section 2 for these two failure modes under indentation and with the support of finite element simulations for parameter identification and/or for validation. The chart corresponding to the two criteria is built and commented in Section 3. Section 4 extends the previous results to the case of scratching.

2. Methods

The system of interest is a thin film of thickness t_f on a thick (here infinitely thick) substrate. The thin layer is assumed to behave in a linear isotropic elastic way with elastic modulus E_f and Poisson ratio ν_f, whereas the soft substrate is considered as linear isotropic elastic-perfectly plastic with von Mises yield locus and with elastic modulus E_s, Poisson ratio ν_s, and yield strength $\sigma_y|_s$. The indentation, abrasion and scratch resistance is modeled as a two-body contact problem where a sphere of radius R indents and scratches the material stack. The sphere represents for instance an abrasive particle of local corresponding curvature $1/R$, a sharp tool in contact with the surface, the tip of an indention test equipment, or the ball of a ball-on-disc test equipment. Perfect adhesion between the film and the substrate is considered.

2.1. Finite element model

Finite element (FE) simulations have been performed using the commercial software Abaqus/Standard in order to guide the development of the analytical solutions and their validation. Without loss of generality, indentation is simulated as a vertical displacement imposed to a rigid sphere of unitary radius using an axisymmetric setting. In order to represent scratching, now within a full 3D setting, a first indentation is performed by imposing a normal load to the rigid sphere. Then, a horizontal displacement is imposed by keeping the previously applied normal load constant. Both the film and the substrate are modeled using CAX8R elements for the axisymmetric indentation simulations and C3D20R elements for scratching simulations. Frictionless contact has been assumed, but some simulations have been performed with friction for comparison. A refined mesh is used in the contact region (see Fig. 1). Rigorous mesh convergence analysis has been performed for both types of models.

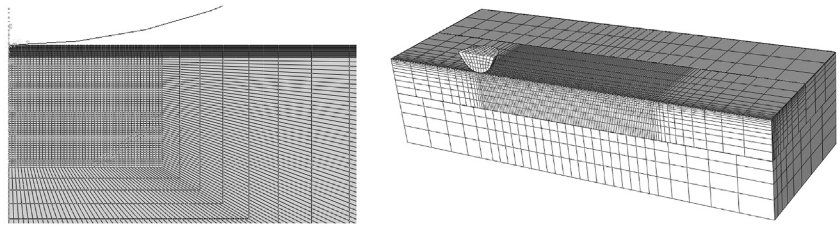

Fig. 1. Detail of the mesh used for the finite element simulations: (left) indentation, (right) scratch. The darker region corresponds to the upper film layer.

A parametric study has been performed for ratio t_f/R ranging from 0.02 to 0.5, film modulus from 100 to 300 GPa, substrate modulus from 0.5 to 4 GPa, and substrate yield strength from 30 to 60 MPa leading to the non-dimensional parameters given in Table 1. Poisson ratio, which plays only a minor role in the problems addressed here, has been fixed equal to 0.2 and to 0.3 for the film and the substrate.

2.2. Analytical contact model

2.2.1. Onset of plastic deformation in the substrate

If the substrate would behave like a non-coated bulk material, the critical force $F_z^{pl}|_{s,\ bulk}$ corresponding to the onset of yielding could be accurately determined by Hertz's relationship as $F_z^{pl}|_{s,bulk} = 21.17\ \frac{R^2}{E_s^{*2}} \sigma_y|_s{}^3$ [31,32]. A comparison of the FE results for the critical force F_z^{pl} for the onset of substrate plastic yielding in the presence of a coating to the theoretical values predicted by the latter Hertz's relationship gives $F_z^{pl}/F_z^{pl}|_{s,\ bulk}$ ratios much higher than one. For instance “Parameter set 5” with $t_f/R = 0.2$ leads to $F_z^{pl}/F_z^{pl}|_{s,bulk} = 85$. Indeed, the stress field in the layered systems significantly differs from the bulk case because the stiff coating distributes the load over a large area in the soft substrate. In the bulk case, the maximum von Mises stress in the substrate $\sigma_{vM,\ max}|_s$ is reached at some distance below the surface whereas in the presence of a hard coating, it is located at the interface. Based on this observation, it is legitimate to assume that $\sigma_{vM,\ max}|_s$ is proportional to the maximum pressure applied to the substrate at the level of the interface.

Since the interest here is about the beginning of the indentation process, the indentation is approximated by a point load. This assumption is valid as far as the contact radius remains small compared to the indentation depth and as far as the phenomena of interest occur sufficiently far from the contact area. In the two elastic foundation models of Winkler and Hogg, the maximum pressure is given by [23–25]:

$$p_{max} = \varphi\ F_z \frac{E_s^{*2/3}}{E_f^{*2/3} t_f^2}, \tag{1}$$

Table 1
Material parameters corresponding to the different parameter sets used in the finite element simulations.

	E_f [GPa]	E_s [GPa]	$\boldsymbol{\sigma_y|_s}$ [MPa]	E_f/E_s	$\boldsymbol{\sigma_y|_s/E_s}$
Parameter set 1	100	2	30	50	0.015
Parameter set 2	200	2	30	100	0.015
Parameter set 3	300	2	30	150	0.015
Parameter set 4	200	2	60	100	0.03
Parameter set 5	200	2	45	100	0.0225
Parameter set 6	200	2	15	100	0.0075
Parameter set 7	200	1	30	200	0.03
Parameter set 8	200	4	30	50	0.0075
Parameter set 9	200	0.5	30	400	0.06
Parameter set 10	200	0.5	60	400	0.12

where $\varphi = 0.268$ and $\varphi = 0.635$ for Winkler's and Hogg's models, respectively. Hence, rewriting (1) by taking into account that yielding of the substrate starts when $\sigma_y|_s = \sigma_{vM,\ max}|_s = \alpha p_{max}$ (with α a proportionality constant), the critical force for the onset of plastic yielding F_z^{pl} can be expressed as follows:

$$F_z^{pl} = \rho \sigma_y\big|_s t_f^2 \frac{E_f^{*\frac{2}{3}}}{E_s^{*\frac{2}{3}}} \text{ or } \frac{F_z^{pl}}{F_z^{pl}\big|_{s,bulk}} = \frac{\rho}{21.17} \frac{t_f}{R} \frac{E_f^{*\frac{1}{3}} E_s^{*\frac{2}{3}}}{\sigma_y\big|_s}^2 \tag{2}$$

where $\rho = 1/(\alpha\varphi)$. Fig. 2 shows, based on the FE results, that the variation of F_z^{pl} with respect to $\sigma_y|_s t_f^2 (E_f^*/E_s^*)^{2/3}$ is indeed linear. The proportionality coefficient ρ extracted from the linear fit of the data of Fig. 2 is equal to 1.268.

2.2.2. Onset of film cracking

The second indentation failure mode of “hard film on soft substrate” systems consists in the cracking of the film. Note that since this analysis considers the first damage mode that will occur, the study is limited to elastically deforming substrate response. Several studies have shown that ring cracks appear at some distance from the contact zone [20–22,28]. These cracks form under tensile stress conditions, which develop from the film surface due to plate bending, as shown in Fig. 3. Outside the contact region, the maximum principal stress is equal to the radial stress σ_r.

Cracking of the film takes place when the stress intensity factor K_I at the tip of a surface flaw becomes larger than the fracture toughness of

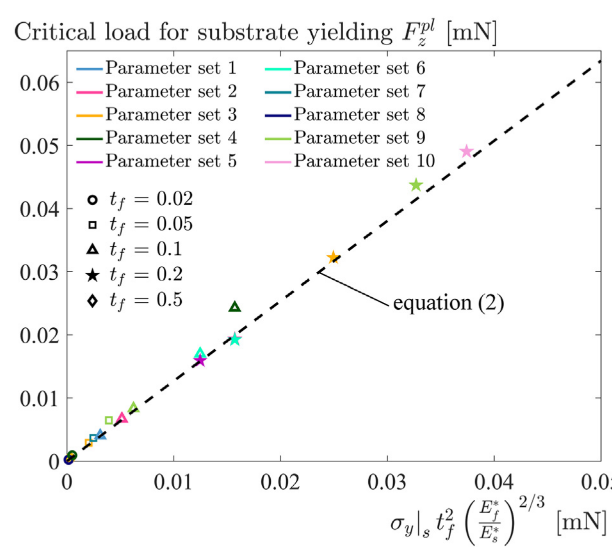

Fig. 2. Variation of the critical force for the onset of substrate yielding in “hard film on soft substrate” systems (from FE calculations, discrete points) as a function of the material properties and dimension combination as suggested by Eq. (2).

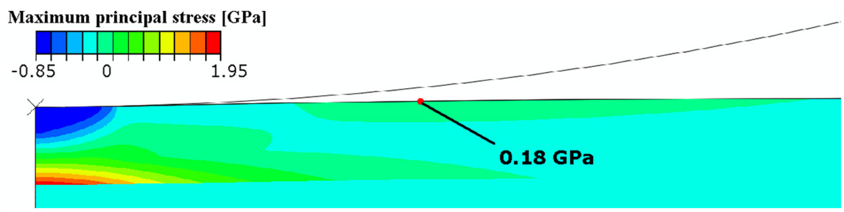

Fig. 3. Maximum principal stress distribution in the hard layer predicted by FE (Parameter set 4 $-t_f/R = 0.02 - F_z/R^2 = 0.9$ MPa). The peak stress at the surface is attained outside the contact area and is oriented radially.

the film. The stress intensity factor of a surface flaw in a film can be related to the applied stress (internal and external) and to the size c of the preexisting flaw [26,27,33]. In particular, Weppelman and Swain [33] proposed the following expression for K_I:

$$K_I(r, F_z, c/t_f) = \int_{\frac{t_f}{2}-c}^{\frac{t_f}{2}} \frac{\sigma_r(r,z,F_z)}{\sqrt{t_f}} w_I(c/t_f, z/t_f)dz \tag{3}$$

where $w_I(c/t_f, z/t_f)$ is a non-dimensional weight function.

Following the plate bending theory, the radial stress σ_r is proportional to the radial curvature $\kappa_r = \frac{\partial^2 u_z}{\partial r^2} + \nu \frac{1}{r}\frac{\partial u_z}{\partial r}$. Hogg's model ends up with the following relationship for the deflection profile [25]:

$$u_z(r) = -F_z \frac{l_H^2}{2\pi D}\left(\frac{r}{l_H}\right)^2 \int_0^\infty \frac{J_0(x)}{x^3 + \left(\frac{r}{l_H}\right)^3} dx \tag{4}$$

where $l_H = (2D/E_s^*)^{1/3}$, $D = E_f^* t_f^3/12$ is the flexural stiffness, $E_f^* = E_f/(1\text{-}\nu_f^2)$ and $E_s^* = E_s/(1\text{-}\nu_f^2)$ are the film and the substrate elastic biaxial modulus, respectively. $J_0(\tau)$ is the 0th order Bessel function of the first kind. One may notice that this load-deflection relationship is the same as the one corresponding to a circular plate made out of the film only and of radius $3.5l_H$. Calculating the second derivative of the surface profile (4) ends up to the following expression for the radial curvature [25]:

$$\kappa_r\left(r, z = \frac{t_f}{2}\right) = \frac{6F_z}{\pi E_f^* t_f^3}\left[\frac{1}{2}\int_0^\infty \frac{x^2(J_2(x) - J_0(x))}{x^3 + \left({r}/{l_H}\right)^3}dx - \nu_f \int_0^\infty \frac{xJ_1(x)}{x^3 + \left({r}/{l_H}\right)^3}dx\right]. \tag{5}$$

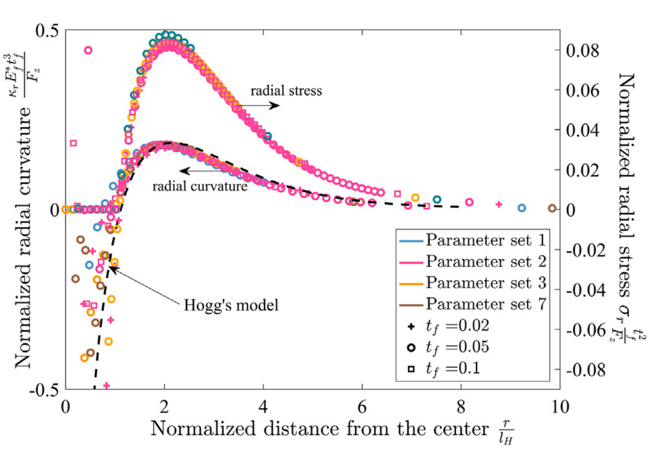

Fig. 4. Variation of the normalized surface curvature and radial stress as a function of the normalized radial distance as predicted by Hogg's model and FE simulations.

Fig. 4 shows the radial curvature calculated by FE simulations from the deflection profile (normalized by $F_z / E_f^* t_f^3$ as suggested by relationship (5)) as a function of the displacement normalized by the characteristic length l_H. Hogg's model provides a fair estimate of the local curvature, even if the maximum extracted from the FE simulations is slightly lower and at slightly smaller r/l_H values. Except near the center of the contact region, the suggested normalization coagulates almost all data into a single curve, especially with respect to the value and location of the maximum curvature. Scatter in the curvature at small r/l_H values is due to the discretization effect in the contact zone and to the numerical double derivation.

In pure bending, the radial stress is related to the radial curvature following the relationship $\sigma_{bend}(r,z) = z\kappa_r(r,z=0)E_f^*$. Still, careful analysis of the FE results shows that the film does not undergo pure bending, but that there is also a small membrane stress component. However, since our analysis is limited to the appearance of the first damage, displacements remain small, and the FE results confirm that the membrane stress can be neglected. Therefore, from pure bending theory and using Eq. (5) for the curvature, the following relationship can be obtained:

$$\sigma_{surf}(r, F_z) \cong \frac{t_f}{2}\kappa_r(r, z=0)E_f^* \cong \frac{t_f}{2}\kappa_r\left(r, z = \frac{t_f}{2}\right)E_f^* = \mu\frac{F_z}{t_f^2} f\left(\frac{r}{l_H}, \nu_f\right), \tag{6}$$

where μ is a proportionality coefficient and $f(r/l_H, \nu_f)$ is a non-dimensional function. Owing to Hogg's model, μ is equal to $3/\pi$ and $f(r/l_H, \nu_f)$ is equal to the expression between brackets in Eq. (5). Fig. 4 confirms that the surface stress scales with F_z/t_f^2. Considering a flaw size distribution $c(r)$, the expression (3) for the stress intensity factor becomes

$$K_I(r, F_z) = \sigma_{surf}(r, F_z)\sqrt{t_f} \int_{\frac{1}{2}-\frac{c(r)}{t_f}}^{\frac{1}{2}} \frac{z}{t_f/2} w_I\left(\frac{c(r)}{t_f}, \frac{z}{t_f}\right) d\left(\frac{z}{t_f}\right). \tag{7}$$

Note that for cases where the film is stiffer than the substrate, it has been shown that the above K_I value is a lower bound, involving a maximum error of 7% [33].

The critical normal load F_z^{crack} at which cracking initiates in the hard coating is the one for which, somewhere in the film, the stress intensity factor reaches the fracture toughness $K_{Ic}|_f$, i.e. F_z^{crack} is equal to the minimum value of F_z for which $\max_{r>0} K_I(r, F_z) = K_{Ic}|_f$. The exact value of F_z^{crack} is dependent on the exact flaw size distribution $c(r)$, which is dependent on the material deposition and operating conditions. Nevertheless, since $w_I(c/t_f, z/t_f)$ is an increasing function of c/t_f, the worst case value for F_z^{crack} corresponds to when the largest crack in the film is located exactly at the position where the radial stress reaches its maximum, i.e. when:

$$K_{Ic}|_f = \max_{r>0} K_I(r, F_z) = \max_{r>0}\left[\sigma_{surf}\left(r, F_z^{crack}\right)\right]\sqrt{t_f}\, g\left(\frac{c_{max}}{t_f}\right), \tag{8}$$

where $g(c/t_f)$ is the result of the integral in (7) and depends only on the relative flaw size $c(r)/t_f$ at a given position. Following Eq. (6), the position r_{max} of the maximum radial stress at the surface $\sigma_{surf}^{max}(F_z)$ is located at the same normalized distance from the center for all sets of parameters and film thicknesses, which is confirmed by Fig. 4. Moreover, the maximum of the radial stress is simply given by

$$\sigma_{surf}^{max}(F_z) = \max_{r>0}\left[\sigma_{surf}\left(r, F_z^{crack}\right)\right] = \gamma\frac{F_z}{t_f^2}. \quad (9)$$

The linear relationship is confirmed by the FE results shown in Fig. 5. Linear interpolation gives a proportionality factor γ equal to 0.0795 whereas Hogg's model (5) predicts $\gamma = \mu \max[f(r/l_H, \nu_f)] = 0.0928$ for $\nu_f = 0.2$.

The critical normal load F_z^{crack} is obtained by inserting this result into Eq. (8):

$$F_z^{crack} = \frac{K_{Ic}|_f t_f^{\frac{3}{2}}}{\gamma g\left(\frac{c_{max}}{t_f}\right)}. \quad (10)$$

In reference [26], the expression for K_I obtained by finite element simulations is $\frac{K_I t_f^{3/2}}{F_z} = (\frac{c}{t_f})^{1/2} h(\frac{c}{t_f}, \frac{E_f}{E_s})$, which is similar to Eq. (7) in terms of parameter dependencies. The only difference is the additional contribution of the ratio E_f/E_s. For small c/t_f ratios, the function h tends to 0.164 and the dependence on the modulus ratio becomes negligible. Compared to Eq. (10), this corresponds to $\gamma\, g(c_{max}/t_f) = 0.164\, (c_{max}/t_f)^{1/2}$. The authors of reference [27] also found the same dependence of K_I on film thickness.

3. Material property charts for indentation resistance

Following Ashby's methodology, material selection maps are built in order to compare the performances of different materials as a function of one or multiple objectives [2]. The position of a material on the chart is given by its "performance index" (also called "index of merit" or "figure of merit") which, ideally, only combines intrinsic properties. Nevertheless, there are some examples where the performance index cannot deconvolute materials, geometry and loading (see e.g. [3]). The performance index, and consequently the charts, depend on the selected objective, which describes the desired end-user behavior. Without loss of generality, the considered objective in the present investigation is to select the material for the thinnest possible film material to coat a given soft substrate. Reasons for this choice of minimizing thickness could be for instance to reduce deposition times, to maintain transparency, to reduce the costs related to material consumption and/or to reduce problems related to stress or property gradients building up during film deposition. However, the approach could be extended to other objectives such as to maximize indentation force or penetration without failure. In the present case, the system must resist indentation under a normal force F_z^* without failure which can be either by substrate yielding or film cracking. Based on relationships (2) and (10), these constraints can be expressed respectively as follows:

$$\log t_f \geq -\frac{1}{2}\log\rho + \frac{1}{2}\log F_z^* - \log\frac{\left(\sigma_y|_s\right)^{\frac{1}{2}}\left(E_f^*\right)^{\frac{1}{3}}}{\left(E_s^*\right)^{\frac{1}{3}}}, \quad (11)$$

$$\log t_f \geq \frac{2}{3}\log F_z^* - \log\left(K_{Ic}|_f\right)^{\frac{2}{3}} + \frac{2}{3}\log\gamma g\left(\frac{c_{max}}{t_f}\right). \quad (12)$$

In a first approach, we assume that all thin film candidates have similar relative maximum pre-existing flaw size c_{max}/t_f. Then, the two performance indices to maximize in order to favor the absence of substrate yielding and film cracking are respectively $I_{pl} = (\sigma_y|_s)^{1/2}\, (E_f^*/E_s^*)^{1/3}$ and $I_{crack} = (K_{Ic}|_f)^{2/3}$. Taking values from the literature for the mechanical properties [34–43], the magnitude of the performance indices of usual thin films have been represented in Fig. 6(a) for the specific case of a typical paint substrate ($E_s^* = 1.1$ GPa and $\sigma_y|_s = 60$ MPa) under an imposed load equal to 75 μN load. Let us mention that materials that can exhibit yielding may still be put on the chart, as far as the fracture of the film or substrate yielding occurs before the film experiences yielding. Note that if the flaw size varies with the film material, then the $\gamma g(c_{max}/t_f)$ term has to be included in the performance index which becomes $I_{crack} = (K_{Ic}|_f\, \gamma\, g(c_{max}/t_f))^{2/3}$. This makes the analysis more complicated as it then directly depends on the deposition conditions and on complex material microstructure evolution aspects. The importance of including size-effects at small scales has already been highlighted by Y. Zou [44].

The minimum film thickness for preventing substrate yielding at F_z^* is represented by horizontal lines. The minimum film thickness for preventing film cracking at F_z^* is represented by vertical lines, whose exact position depends on the relative flaw size c_{max}/t_f. Combining (11) and (12) and using $\gamma g(c_{max}/t_f) = 0.164\, (c_{max}/t_f)^{1/2}$ gives the following equation:

$$\log I_{pl} = -\frac{1}{2}\log\rho - \frac{2}{3}\log 0.164 - \frac{1}{6}\log F_z^* - \frac{1}{3}\log\frac{c_{max}}{t_f} + \log I_{crack}. \quad (13)$$

This line represents all the couples (I_{crack}, I_{pl}), which, for a given F_z^*, lead to the same minimum film thickness for the two failure modes. Since either mode induces failure, the largest thickness is used to determine the film thickness. All points above the line set by Eq. (13) correspond to materials for which the controlling failure mode is film cracking, whereas all points below the line set by Eq. (13) correspond to materials for which the controlling failure mode is substrate yielding. Therefore, isoperformance lines are L-shaped curves with the corner located on the adequate c_{max}/t_f line given by Eq. (13). For instance, for the present substrate properties ($E_s^* = 1.1$ GPa and $\sigma_y|_s = 60$ MPa), neither of the two considered failure modes will appear under a load of 75 μN if a 0.2 μm thick SiN_x film is deposited. On the other hand, the same load will lead to substrate yielding if the film is a 0.2 μm thick SiO_2 or Al_2O_3. The best material is obtained by shifting the L-shaped curve along line set by (13) until only one is left. In the present case, it would be ultra-nanocrystalline diamond (UNCD) while SiO_2 would be the worst one. Diamond and UNCD emerge as the best materials. However, one may prefer to minimize deposition costs instead of film

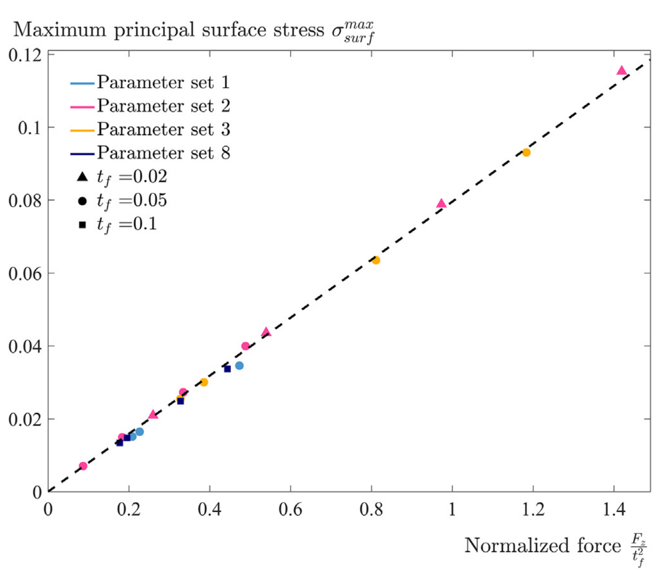

Fig. 5. Variation of the maximum principal stress at the surface as a function of the normalized force F_z/t_f^2.

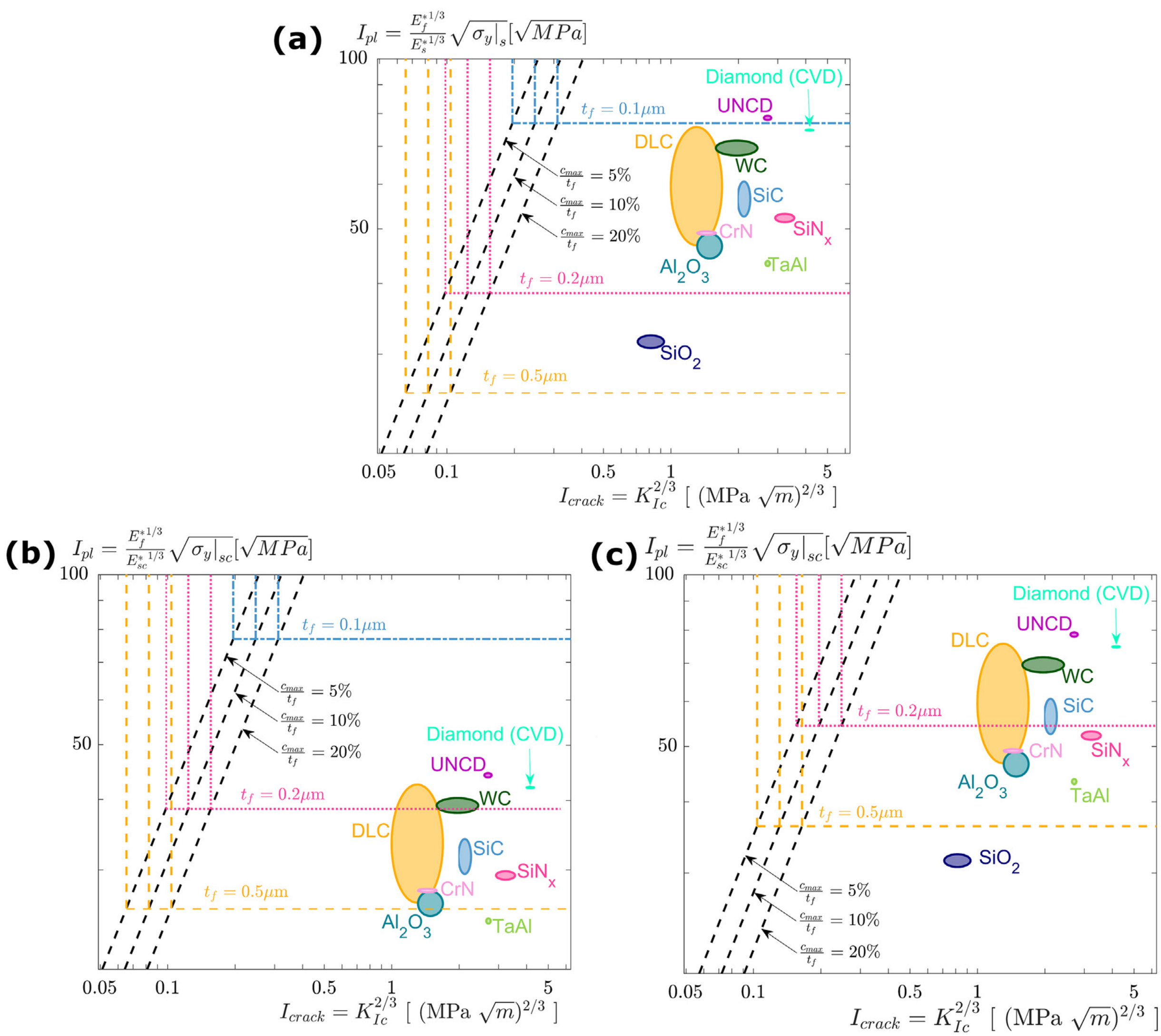

Fig. 6. Property map for the resistance to film cracking and yielding under normal blunt contacts for a substrate characterized with (a) $E_s^* = 1.1$ GPa and $\sigma_y|_s = 60$ MPa and 75 μN applied load; (b) $E_s^* = 2.2$ GPa and $\sigma_y|_s = 30$ MPa and 75 μN applied load; (c) $E_s^* = 1.1$ GPa and $\sigma_y|_s = 60$ MPa and 150 μN applied load. The vertical and horizontal axes are the same on all figures to allow comparison.

thickness. Then, deposition price will appear in the performance index and other materials may emerge as better choices.

From Fig. 6, it may be noted that for the considered films, the only failure mode is by substrate yielding. This may seem surprising given the number of experimental results where film cracking has been observed. This is related to the fact that, here, we considered the onset of substrate yielding as a critical damage mode. The relevance of this choice is highly dependent on the application. For instance, one may accept some degree of substrate yielding as far as the residual imprint is less than a certain depth. Then, of course, the performance index corresponding to the latter damage will differ from the above one, and the cracking resistance may become critical. In addition, the analysis does not take internal stresses into account, although frequently present found in thin films and coatings. Equibiaxial internal tensile stresses will favor film cracking.

Generalization of the chart presented in Fig. 6(a) to other substrates or to other loads is very easy. Indeed, changing the substrate implies other values of E_s^* and $\sigma_y|_s$. This will lead to a vertical shift of the position of the different materials on the chart, whereas the isoperformance lines remain unchanged, as it can be seen on the example of Fig. 6(b). On the contrary, changing the value of the normal force will lead to a vertical shift of the isoperformance lines while the position of the different materials on the chart remains constant, as it can be seen in Fig. 6(c).

Finally, let us mention that, although all simulations have been performed with a spherical indenter (i.e. a blunt contact), the radius of the tip does not appear in the performance indices. This is because, in the proposed model, the indent is considered as a point load. Therefore, the proposed performance indices and hence the proposed charts are also valid for a sharp contact.

4. From indentation to scratch resistance

Coatings are often applied not only for protection against indentation, but also against scratch induced damage. Scratching and penetration are closely related. Scratch may be seen as a combination of a normal indentation with a lateral displacement of the tip [45]. In all further analysis, scratch data are taken when the steady state response is attained. The FE results show that for hard brittle film on soft substrate systems, the penetration depth during scratching is almost the same as for indentation under the same load.

Similarly, Fig. 7 shows that the maximum radial stress at the film surface during scratching is proportional to the value obtained during indentation. Even more, the proportionality factor is almost equal to one, since linear interpolation of the FE simulation results gives a slope of 1.084. In the same way, Fig. 7 compares also $\sigma_{vM,\ max}|_s$ during

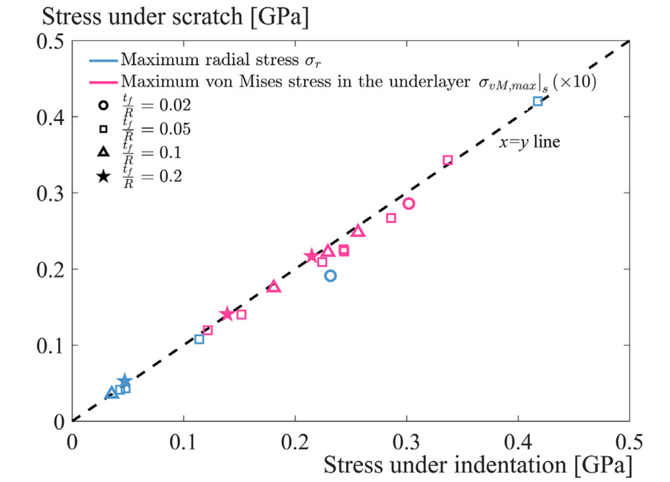

Fig. 7. Comparison between indentation and during scratching under the same load of maximum radial stress in front of the tip and of maximum von Mises stress in the substrate during.

indentation and during scratching. Again, $\sigma_{vM,\ max}|_s$ during scratching is almost equal to the one during indentation.

Hence, critical loads for film cracking and substrate yielding during indentation are representative of the critical loads during scratching. Friction between the indenter and coating strongly affects the stress distributions under contact during sliding, which would then differ from the values during indentation. However, since we are considering only small indentation depths, the contact area remains small and the influence of friction is limited. Some FE simulations with a friction coefficient of 0.2 have been performed, and the resulting maximum stress values differ by <2%.

The performance indices developed in Section 3 can therefore also be used for classifying the films with respect to the crack resistance during scratching. This is a very important conclusion as long as no other failure mode such as interfacial decohesion plays a role. Indeed, in the latter case, the system will react differently under indentation or scratch loading conditions. Another important point is that this study only predicts circular crack patterns. Similar to the indentation case, one may accept some degree of substrate yielding as far as the residual groove is less than a certain depth. Then, other crack patterns may arise before the ring cracks in front of the tip, such as angular cracks. These other crack configurations result from the addition of groove edge bending effects when a permanent groove is formed due to plastic deformation [46].

5. Conclusion

The mechanical framework developed by Zok et al. [1] for indentation and abrasion resistance of bulk materials has been extended to the case of layered "hard film on soft substrate" systems for blunt or sharp contacts without friction. A simple model for estimating indentation stresses in the film-substrate system as a function of material properties has been developed and validated by FE simulations. For the considered failure modes, the stress field generated during indentation or by scratching are almost identical.

The main finding of this work is the formulation of performance indices for the resistance to film cracking and substrate yielding, which have been derived from the abovementioned models. These performance indices show that taking the hardest possible coating is not always the best choice, as the stiffness and the fracture toughness also play a role. The results are presented in the form of selection charts, which aim at classifying different (film-substrate) couples with respect to the resistance to failure. Depending on the way the charts are generated, they can be used either for selecting the best film for a given substrate, the best substrate for a given film or the best (film-substrate) couple for a given selection of (film-substrate) combinations. The findings of this work could be also applicable to ball-on-disc testing conditions. Due to uncertainties on flaw dimensions as related to the film material and deposition conditions, these charts remain however mainly a guide to think and orient developments rather than an absolute and definitive decision-making support. Another element that has not been taken into account is the presence of internal stress, which can be introduced in a straightforward way in the models proposed in the present study.

Nevertheless, this is only a first step towards an efficient selection tool for coated systems. Indeed, due to the presence of more than one material, the number of possible failure modes is larger than in bulk materials: any of the materials can fail, as well as interfaces. Simple models for critical failure forces or displacements, which can be translated to performance indices, have to be developed. Also, the opposite case to the one studied here, i.e. "soft-layer-on-hard-substrate" is of major interest and currently under investigation. In this case, pile-up formation and delamination are two major damage modes.

Author credit statement

Audrey Favache is the main researcher and main author of this work. Alain Daniel and Aline Teillet are co-workers of the research project, and provided ideas during the research, as well as experimental samples and data. They also reviewed the manuscript before submission. Pr. Thomas Pardoen provided project management and consultation (including in-depth review and enhancement of the manuscript before submission and revision).

Acknowledgements

The authors acknowledge the financial support of the Walloon Region through the CARUSO project (convention no. 1410076). Computational resources have been provided by the Consortium des Équipements de Calcul Intensif (CÉCI), funded by the Fonds de la Recherche Scientifique de Belgique (F.R.S.-FNRS) under Grant No. 2.5020.11 and by the Walloon Region.

Data availability

The raw/processed data required to reproduce these findings cannot be shared at this time due to legal or ethical reasons.

References

[1] F.W. Zok, A. Miserez, Property maps for abrasion resistance of materials, Acta Mater. 55 (2007) 6365–6371, https://doi.org/10.1016/j.actamat.2007.07.042.
[2] M.F. Ashby, Materials Selection in Mechanical Design, 4th ed. Pergamon Press, 2010.
[3] I. Huynen, N. Quiévy, C. Bailly, P. Bollen, C. Detrembleur, S. Eggermont, I. Molenberg, J.M. Thomassin, L. Urbanczyk, T. Pardoen, Multifunctional hybrids for electromagnetic absorption, Acta Mater. 59 (2011) 3255–3266, https://doi.org/10.1016/j.actamat.2011.01.065.
[4] Z. Mehmood, I. Haneef, F. Udrea, Material selection for Micro-Electro-Mechanical-Systems (MEMS) using Ashby's approach, Mater. Des. 157 (2018) 412–430, https://doi.org/10.1016/j.matdes.2018.07.058.
[5] E.T. Bird, A.E. Bowden, M.K. Seeley, D.T. Fullwood, Materials selection of flexible open-cell foams in energy absorption applications, Mater. Des. 137 (2018) 414–421, https://doi.org/10.1016/j.matdes.2017.10.054.
[6] R.A. Antunes, C.A.F. Salvador, M.C.L. de Oliveira, Materials selection of optimized titanium alloys for aircraft applications, Mater. Res. 21 (2018)https://doi.org/10.1590/1980-5373-mr-2017-0979.
[7] M.M. Falinski, D.L. Plata, S.S. Chopra, T.L. Theis, L.M. Gilbertson, J.B. Zimmerman, A framework for sustainable nanomaterial selection and design based on performance, hazard, and economic considerations, Nat. Nanotechnol. 13 (2018) 708–714, https://doi.org/10.1038/s41565-018-0120-4.
[8] Y. Su, Z. Liu, S. Wang, R. Ghaffari, D.-H. Kim, K.-C. Hwang, J.A. Rogers, Y. Huang, Mechanics of stretchable electronics on balloon catheter under extreme deformation, Int. J. Solids Struct. 51 (2014) 1555–1564.
[9] J. Caro, N. Cuadrado, I. González, D. Casellas, J.M. Prado, A. Vilajoana, P. Artús, S. Peris, A. Carrilero, J.C. Dürsteler, Microscratch resistance of ophthalmic coatings on organic

lenses, Surf. Coat. Technol. 205 (2011) 5040–5052, https://doi.org/10.1016/j.surfcoat.2011.05.006.
[10] S.J. Bull, Failure modes in scratch adhesion testing, Surf. Coat. Technol. 50 (1991) 25–32.
[11] K. Holmberg, A. Matthews, Coatings Tribology: Properties, Mechanisms, Techniques and Applications in Surface Engineering, 2nd ed. Elsevier, 2009.
[12] Z. Chen, L.Y.L. Wu, E. Chwa, O. Tham, Scratch resistance of brittle thin films on compliant substrates, Mater. Sci. Eng. A 493 (2008) 292–298, https://doi.org/10.1016/j.msea.2007.07.099.
[13] A. Favache, C.-H. Sacré, M. Coulombier, L. Libralesso, P. Guaino, J.-P. Raskin, C. Bailly, B. Nysten, T. Pardoen, Fracture mechanics based analysis of the scratch resistance of thin brittle coatings on a soft interlayer, Wear (2015) 330–331, https://doi.org/10.1016/j.wear.2015.01.081.
[14] C.H. Sacré, F. Lani, P. Guaino, L. Libralesso, A. Favache, T. Pardoen, Effect of polymer interlayer on scratch resistance of hard film: experiments and finite element modeling, Wear 378–379 (2017)https://doi.org/10.1016/j.wear.2017.02.033.
[15] M.R. McGurk, T.F. Page, Exploration of the plate bending model for predicting the hardness response of coated systems, Surf. Coat. Technol. 92 (1997) 87–95, https://doi.org/10.1016/S0257-8972(97)00012-1.
[16] A.M. Korsunsky, M.R. McGurk, S.J. Bull, T.F. Page, On the hardness of coated systems, Surf. Coat. Technol. 99 (1998) 171–183http://www.sciencedirect.com/science/article/pii/S0257897297005227.
[17] S.J. Bull, Nanoindentation of coatings, J. Phys. D. Appl. Phys. 38 (2005) 393–413, https://doi.org/10.1088/0022-3727/38/24/R01.
[18] A. Iost, G. Guillemot, Y. Rudermann, M. Bigerelle, A comparison of models for predicting the true hardness of thin films, Thin Solid Films 524 (2012) 229–237, https://doi.org/10.1016/j.tsf.2012.10.017.
[19] W.W. Gerberich, A. Strojny, K. Yoder, L.S. Cheng, Hard protective overlayers on viscoelastic-plastic substrates, J. Mater. Res. 14 (1999) 2210–2218.
[20] D.F. Bahr, C.L. Woodcock, M. Pang, K.D. Weaver, N.R. Moody, Indentation induced film fracture in hard film-soft substrate systems, Int. J. Fract. 120 (2003) 339–349, https://doi.org/10.1023/A:1024979030155.
[21] N.G. Chechenin, J. Bøttiger, J.P. Krog, Nanoindentation of amorphous aluminum oxide films I. The influence of the substrate on the plastic properties, Thin Solid Films 261 (1995) 219–227, https://doi.org/10.1016/S0040-6090(94)06490-3.
[22] N.G. Chechenin, J. Bøttiger, J.P. Krog, Nanoindentation of amorphous aluminum oxide films II. Critical parameters for the breakthrough and a membrane effect in thin hard films on soft substrates, Thin Solid Films 261 (1995) 228–235, https://doi.org/10.1016/S0040-6090(94)06494-6.
[23] E. Winkler, Die Lehre von der Elasticitaet und Festigkeit mit besonderer Rücksicht auf ihre Anwendung in der Technik: für polytechnische Schulen, Bauakademien, Ingenieure, Maschinenbauer, Architecten, etc., Dominicius, Prag, 1867.
[24] S. Timoshenko, S. Woinowsky-Krieger, Theory of Plates and Shells, 2nd ed. McGraw-Hill, 1987.
[25] A.H.A. Hogg, XLVIII. Equilibrium of a thin plate, symmetrically loaded, resting on an elastic foundation of infinite depth, London, Edinburgh, Dublin Philos. Mag. J. Sci. 25 (1938) 576–582, https://doi.org/10.1080/14786443808562039.
[26] H. Chai, Fracture mechanics analysis of thin coatings under spherical indentation, Int. J. Fract. 119 (2003) 263–285.
[27] K. Sriram, R. Narasimhan, S.K. Biswas, A numerical fracture analysis of indentation into thin hard films on soft substrates, Eng. Fract. Mech. 70 (2003) 1323–1338, https://doi.org/10.1016/S0013-7944(02)00112-1.
[28] D. Mercier, V. Mandrillon, G. Parry, M. Verdier, R. Estevez, Y. Bréchet, T. Maindron, Investigation of the fracture of very thin amorphous alumina film during spherical nanoindentation, Thin Solid Films 638 (2017) 34–47, https://doi.org/10.1016/j.tsf.2017.07.040.
[29] S.J. Bull, Failure mode maps in the thin film scratch adhesion test, Tribol. Int. 30 (1997) 491–498.
[30] A. Chauhan, R. Vaish, Hard coating material selection using multi-criteria decision making, Mater. Des. 44 (2013) 240–245, https://doi.org/10.1016/j.matdes.2012.08.003.
[31] H. Hertz, Über die Berührung fester elastischer Körper, J. Für Die Reine Und Angew. Math. 92 (1881) 156–171.
[32] K.L. Johnson, Contact Mechanics, Cambridge University Press, 2003.
[33] E. Weppelmann, M.V. Swain, Investigation of the stresses and stress intensity factors responsible for fracture of thin protective films during ultra-micro indentation tests with spherical indenters, Thin Solid Films 286 (2006) 111–121.
[34] D.C. Miller, R.R. Foster, Y. Zhang, S.-H. Jen, J.A. Bertrand, Z. Lu, D. Seghete, J.L. O'Patchen, R. Yang, Y.-C. Lee, S.M. George, M.L. Dunn, The mechanical robustness of atomic-layer- and molecular-layer-deposited coatings on polymer substrates, J. Appl. Phys. 105 (2009), 093527.
[35] A. van der Rest, H. Idrissi, F. Henry, A. Favache, D. Schryvers, J. Proost, J.-P. Raskin, Q. Van Overmeere, T. Pardoen, Mechanical behavior of ultrathin sputter deposited porous amorphous Al2O3 films, Acta Mater. 125 (2017) 27–37, https://doi.org/10.1016/j.actamat.2016.11.037.
[36] R. Pastorelli, A.C. Ferrari, M.G. Beghi, C.E. Bottani, J. Robertson, Elastic constants of ultrathin diamond-like carbon films, Diam. Relat. Mater. 9 (2000) 825–830, https://doi.org/10.1016/S0925-9635(99)00245-9.
[37] J.J. Bellante, H. Kahn, R. Ballarini, C. Zorman, M. Mehregany, A.H. Heuer, Fracture Toughness of Polycrystalline Silicon Carbide Thin Films, 2005https://doi.org/10.1063/1.1864246.
[38] B. Merle, M. Göken, Fracture Toughness of Silicon Nitride Thin Films of Different Thicknesses as Measured by Bulge Tests, 2011https://doi.org/10.1016/j.actamat.2010.11.043.
[39] V. Hatty, H. Kahn, A.H. Heuer, Fracture toughness, fracture strength, and stress corrosion cracking of silicon dioxide thin films, J. Microelectromech. Syst. 17 (2008) 943–947, https://doi.org/10.1109/JMEMS.2008.927069.
[40] S. Zhang, D. Sun, Y. Fu, H. Du, Toughness measurement of thin films: a critical review, Surf. Coat. Technol. 198 (2005) 74–84http://www.sciencedirect.com/science/article/pii/S0257897204010084.
[41] Y. Xiang, J. McKinnell, W.-M. Ang, J.J. Vlassak, Measuring the fracture toughness of ultra-thin films with application to AlTa coatings, Int. J. Fract. 144 (2007) 173–179, https://doi.org/10.1007/s10704-007-9095-0.
[42] N. Pugno, B. Peng, H.D. Espinosa, Predictions of strength in MEMS components with defects––a novel experimental–theoretical approach, Int. J. Solids Struct. 42 (2005) 647–661.
[43] A. Favache, L. Libralesso, P.J. Jacques, J.-P. Raskin, C. Bailly, B. Nysten, T. Pardoen, Fracture toughness measurement of ultra-thin hard films deposited on a polymer interlayer, Thin Solid Films 550 (2014) 464–471, https://doi.org/10.1016/j.tsf.2013.10.052.
[44] Y. Zou, Materials selection in micro- or nano-mechanical design: towards new Ashby plots for small-sized materials, Mater. Sci. Eng. A 680 (2017) 421–425, https://doi.org/10.1016/j.msea.2016.10.123.
[45] S.E. Flores, M.G. Pontin, F.W. Zok, Scratching of elastic/plastic materials with hard spherical indenters, J. Appl. Mech. 75 (2008) 0610211–0610217, https://doi.org/10.1115/1.2966268.
[46] K. Holmberg, A. Laukkanen, H. Ronkainen, K. Wallin, S. Varjus, A model for stresses, crack generation and fracture toughness calculation in scratched TiN-coated steel surfaces, Wear 254 (2003) 278–291http://www.sciencedirect.com/science/article/B6V5B-47P1TSN-1/2/edeefd3b2141b1901aac3d8054859659.